Conditions for Stability of Droop–Controlled Inverter–Based Microgrids

Johannes Schiffer[a,*], Romeo Ortega[b], Alessandro Astolfi[c], Jörg Raisch[a,d], Tevfik Sezi[e]

[a] *Technische Universität Berlin, Einsteinufer 11, 10587 Berlin, Germany*
[b] *Laboratoire des Signaux et Systémes, École Supérieure d'Electricité (SUPELEC), Gif-sur-Yvette 91192, France*
[c] *Department of Electrical and Electronic Engineering, Imperial College London, London SW7 2AZ, U.K. & Dipartimento di Ing. Civile e Ing. Informatica, University of Rome, Tor Vergata, 00133 Rome, Italy*
[d] *Max-Planck-Institut für Dynamik komplexer technischer Systeme, Sandtorstr. 1, 39106 Magdeburg, Germany*
[e] *Siemens AG, Smart Grid Division, Energy Automation, Humboldtstr. 59, 90459 Nuremberg, Germany*

Abstract

We consider the problem of stability analysis for droop–controlled inverter–based microgrids with meshed topologies. The inverter models include variable frequencies as well as voltage amplitudes. Conditions on the tuning gains and setpoints for frequency and voltage stability, together with desired active power sharing, are derived in the paper. First, we prove that for all practical choices of these parameters global boundedness of trajectories is ensured. Subsequently, assuming the microgrid is lossless, a port–Hamiltonian description is derived, from which sufficient conditions for stability are given. Finally, we propose for generic lossy microgrids a design criterion for the controller gains and setpoints such that a desired steady–state active power distribution is achieved. The analysis is validated via simulation on a microgrid based on the CIGRE (Conseil International des Grands Réseaux Electriques) benchmark medium voltage distribution network.

Keywords: microgrid control, microgrid stability, smart grid applications, inverters, droop control, port–Hamiltonian systems, power sharing

1. Introduction

Motivated by environmental, economic and technological aspects, the penetration of renewable energy sources into the electrical networks is increasing worldwide. Most of these sources are small–scale distributed generation (DG) units connected at the low voltage (LV) and medium voltage (MV) levels via alternating current (AC) inverters. As a consequence, the power generation structure is moving from purely large, centralized plants to a mixed generation pool consisting of conventional large plants and smaller distributed generation units. Since, in addition, the physical characteristics of inverters largely differ from the characteristics of conventional electrical generators (*i.e.* synchronous generators (SGs)), new concepts and strategies to operate the electric power system that ensure a reliable and stable operation are needed.

The microgrid concept represents one promising solution to address these issues by facilitating local integration of renewable energy sources [25, 18]. In general, a microgrid gathers a combination of generation units, loads and energy storage elements at distribution level into a locally controllable system, which can be operated in a decentralized and completely isolated manner from the main transmission system. An autonomous or islanded microgrid is operated in such mode. The microgrid concept has been identified as a key component in future electrical networks [11]. Furthermore, it is envisioned to greatly contribute to the implementation of numerous smart grid functions [26].

In this work we consider three important problems in such networks: frequency stability, voltage stability and power sharing. Power sharing is understood as the ability of the local controllers of the individual generation sources to achieve a desired steady–state distribution of their power outputs *relative* to each other, while satisfying the load demand in the network. The relevance of this control objective lies within the fact that it allows to prespecify the utilization of the generation units in operation.

A control technique widely used to address the problem of active power sharing in large power systems is droop control, also referred to as power–speed characteristic [23]. In droop control the current value of the rotational speed of each SG in the network is monitored locally to derive how much mechanical power each SG needs to provide.

*Corresponding author J. Schiffer. Tel. +49-30-314-23573. Fax +49-30-314-21137.
Email addresses: schiffer@control.tu-berlin.de (Johannes Schiffer), ortega@lss.supelec.fr (Romeo Ortega), a.astolfi@ic.ac.uk (Alessandro Astolfi), raisch@control.tu-berlin.de (Jörg Raisch), tevfik.sezi@siemens.com (Tevfik Sezi)

From a control perspective, droop control is a decentralized proportional controller where the control gain (known as droop gain) specifies the steady–state power distribution in the network. Since performance under droop control is satisfactory for large SG–based systems, this technique has been adapted to inverter–based grids [3, 4, 40, 1].

In large SG–based transmission systems droop control is usually only applied to obtain a desired active power distribution, while the voltage amplitude at a generator bus is regulated to a nominal voltage setpoint via an automatic voltage regulator (AVR) acting on the excitation system of the SG. In microgrids the power lines are typically relatively short. Then, the AVR employed at the transmission level is, in general, not appropriate because slight differences in voltage amplitudes can cause high reactive power flows. As a consequence, the reactive power sharing among generation units cannot be ensured. Therefore, droop control is typically applied in microgrids to achieve also a desired reactive power distribution. The most common approach is to control the voltage amplitude with a proportional control, the feedback signal of which is the reactive power generation relative to a reference setpoint [3, 4]. See the recent survey [15] for further details.

The paper is devoted to the stability analysis of droop–controlled microgrids operated with the control laws given in [3]. These droop control laws are heuristic control laws derived under the assumption of a dominantly inductive network, *i.e.* for power lines with small R/X ratios, and they are (by far) the most commonly used ones in this scenario. If the network lines possess large resistive components, the standard droop control exhibits limitations [15]. In this case, several modified droop controls [6, 43, 16] have been proposed. Even in the presence of non–negligible line resistances the application of the droop controls of [3, 4] can be justified, on one hand, via the virtual impedance approach [17] while, on the other hand, invoking their analogy to conventional droop control [10] of SG–based grids.

As in any conventional power system, stability is understood in the sense of achieving asymptotic synchronization of the frequencies of all DG units, with the angle differences not exceeding $|\frac{\pi}{2}|$ and constant generated voltages [24]. Since the synchronization frequency is the same for all DG units and their dynamics depend on the angle differences, it is possible to translate—via a time–dependent coordinate shift—the synchronization objective into a (standard) equilibrium stabilization problem, which is the approach adopted in the paper.

Stability analysis of droop–controlled microgrids has traditionally been carried out by means of detailed numerical small–signal analysis as well as extensive simulations and experimental studies aiming to characterize a range for the droop gains guaranteeing system stability [4, 40, 32, 1]. As pointed out in [15], most work on microgrid stability has so far focussed on radial microgrids, while stability of microgrids with meshed topologies and decentralized controlled units is still an open research area. For radial lossless microgrids, and under the assumption of constant voltage amplitudes, analytic conditions for proportional power sharing and synchronization of lossless microgrids with first–order inverter models has been recently derived – applying results of the theory of coupled oscillators – in [38]. Conditions for voltage stability for a lossless parallel microgrid with one common load have been derived in [39].

For general meshed networks, with the aim to schedule the droop coefficients under the consideration of frequency droop, an iterative procedure based on bifurcation theory has been proposed in [7]. Under the assumption of constant voltage amplitudes, analytic synchronization conditions for a lossy meshed microgrid with distributed rotational and electronic generation are derived in [36] using ideas from second order consensus algorithms. A decentralized LMI–based control design for lossy meshed inverter–based networks guaranteeing overall network stability for a nonlinear model considering variable voltage amplitudes and phase angles, while accounting for power sharing, is provided in [35].

The main contribution of the present paper is to give conditions on the droop gains to ensure stability of droop–controlled inverter–based microgrids with general meshed topology and inverter models with variable frequencies as well as variable voltage amplitudes. In contrast to [38, 39, 36], no assumptions of constant voltage amplitudes or small phase angle differences are made. In this more general scenario, the graph theoretic methods employed in the aforementioned papers are not directly applicable. Instead, we adopt a classical Lyapunov–like approach for analysis of stability of equilibria and boundedness of trajectories. Following the interconnection and damping assignment passivity–based control approach [30, 37], we represent the lossless microgrid system in port–Hamiltonian form [34] to identify the energy–Lyapunov function and give conditions for stability of the frequency synchronization equilibrium state.

The present work extends our results in [37] in several regards: first, conditions for global boundedness are given for lossy microgrids; second, we relate the spectral properties of the local network couplings between the phase angles and the active power flows of the microgrid in port–Hamiltonian form (which has a reduced state vector in relative coordinates) to those of the microgrid in absolute coordinates; third, making use of the global boundedness result, a relaxed stability condition for a lossless microgrid under a specific parameter selection of the controller gains and setpoints of the frequency droop control is derived; finally, the theoretical analysis is illustrated via detailed simulation scenarios.

The remainder of the paper is organized as follows. The network model is presented in Section 2. In Section 3 we give the model of the inverter and the droop control. Section 4 presents conditions for global boundedness of trajectories. Sufficient conditions for stability for lossless microgrids are established in Section 5. In Section 6 we

propose a selection of the droop gains and setpoints, similar to the one given in [38], that ensures the DG units share (in steady–state) the active power according to a specified pattern. Compared to [38], we extend the proof to lossy networks, *i.e.* networks with nonzero conductances. Our analysis is validated in Section 7 with simulation examples based on the CIGRE (Conseil International des Grands Réseaux Electriques) benchmark MV distribution network [33]. The paper is wrapped–up with some conclusions and discussion of future work in Section 8.

Notation We define the sets $\bar{n} := \{1, \dots, n\}$, $\mathbb{R}_{\geq 0} := \{x \in \mathbb{R} | x \geq 0\}$, $\mathbb{R}_{>0} := \{x \in \mathbb{R} | x > 0\}$ and $\mathbb{S} := [0, 2\pi)$. Given a set $\mathcal{U} := \{\nu_1, \dots, \nu_n\}$, the notation $i \sim \mathcal{U}$ denotes "for all $i \in \mathcal{U}$". Let $x := \mathrm{col}(x_i) \in \mathbb{R}^n$ denote a vector with entries x_i for $i \sim \bar{n}$, $\underline{0}_n \in \mathbb{R}^n$ the zero vector, $\mathbb{1}_n \in \mathbb{R}^n$ the vector with all entries equal to one, I_n the $n \times n$ identity matrix, $0_{n\times n}$ the $n \times n$ matrix with all entries equal to zero and $\mathrm{diag}(a_i), i = 1, \dots n$ an $n \times n$ diagonal matrix with diagonal entries a_i. Given a matrix $A \in \mathbb{R}^{n\times n}$ let $\sigma(A)$ denote its spectrum. Let j denote the imaginary unit. Finally, ∇f denotes the transpose of the gradient of a function $f : \mathbb{R}^n \to \mathbb{R}$.

2. Network model

We consider a generic meshed microgrid and, following the classical approach in conventional power system studies, assume that loads are modeled by constant impedances [41]. This leads to a set of nonlinear differential–algebraic equations. Then a network reduction (called Kron reduction [23]) is carried out to eliminate all algebraic equations corresponding to loads and obtain a set of differential equations. We assume this process has been carried out and work with the Kron–reduced network.

The Kron–reduced microgrid is formed by $n \geq 1$ nodes, each of which represents a DG unit interfaced via an AC inverter. We denote the set of network nodes by $\bar{n}$ and associate a time–dependent phase angle $\delta_i : \mathbb{R}_{\geq 0} \to \mathbb{S}$, as well as a voltage amplitude $V_i : \mathbb{R}_{\geq 0} \to \mathbb{R}_{>0}$ to each node $i \in \bar{n}$ in the microgrid. Two nodes i and k of the microgrid are connected via a complex nonzero admittance $Y_{ik} := G_{ik} + jB_{ik} \in \mathbb{C}$ with conductance $G_{ik} \in \mathbb{R}$ and susceptance $B_{ik} \in \mathbb{R}$. For convenience, we define $Y_{ik} := 0$ whenever i and k are not directly connected. The set of neighbors of a node $i \in \bar{n}$ is denoted by $\mathcal{N}_i := \{k \mid k \in \bar{n},\ k \neq i\ , Y_{ik} \neq 0\}$. For ease of notation, we write angle differences as $\delta_{ik} := \delta_i - \delta_k$.

We assume that the microgrid is connected, *i.e.* that for all pairs $\{i, k\} \in \bar{n} \times \bar{n}$, $i \neq k$, there exists an ordered sequence of nodes from i to k such that any pair of consecutive nodes in the sequence are connected by a power line represented by an admittance. This assumption is reasonable for a microgrid, unless severe line outages separating the system into several disconnected parts occur.

The active and reactive power flows $P_{ik} : \mathbb{S}^2 \times \mathbb{R}^2_{>0} \to \mathbb{R}$ and $Q_{ik} : \mathbb{S}^2 \times \mathbb{R}^2_{>0} \to \mathbb{R}$ from node $i \in \bar{n}$ to node $k \in \bar{n}$ are then given by [23]

$$\begin{aligned} P_{ik}(t) =& G_{ik}V_i^2(t) \\ &- V_i(t)V_k(t)(G_{ik}\cos(\delta_{ik}(t)) + B_{ik}\sin(\delta_{ik}(t))), \\ Q_{ik}(t) =& -B_{ik}V_i^2(t) \\ &- V_i(t)V_k(t)(G_{ik}\sin(\delta_{ik}(t)) - B_{ik}\cos(\delta_{ik}(t))). \end{aligned}$$

The overall active and reactive power flows $P_i : \mathbb{S}^n \times \mathbb{R}^n_{>0} \to \mathbb{R}$ and $Q_i : \mathbb{S}^n \times \mathbb{R}^n_{>0} \to \mathbb{R}$ at a node $i \in \bar{n}$ are obtained as[1]

$$\begin{aligned} P_i =& G_{ii}V_i^2 - \sum_{k\sim\mathcal{N}_i} V_iV_k(G_{ik}\cos(\delta_{ik}) + B_{ik}\sin(\delta_{ik})), \\ Q_i =& -B_{ii}V_i^2 - \sum_{k\sim\mathcal{N}_i} V_iV_k(G_{ik}\sin(\delta_{ik}) - B_{ik}\cos(\delta_{ik})), \end{aligned} \tag{1}$$

with

$$G_{ii} := \hat{G}_{ii} + \sum_{k\sim\mathcal{N}_i} G_{ik},\ B_{ii} := \hat{B}_{ii} + \sum_{k\sim\mathcal{N}_i} B_{ik}, \tag{2}$$

where $\hat{G}_{ii} \in \mathbb{R}$ and $\hat{B}_{ii} \in \mathbb{R}$ denote the shunt conductance, respectively shunt susceptance, at node i. The apparent power flow is given by $S_i = P_i + jQ_i$.

Since we are mainly concerned with dynamics of generation units, we express all power flows in "Generator Reference Arrow System" [12].

3. Modeling of inverters and droop control

We model the inverters as AC voltage sources the amplitude and frequency of which can be defined by the designer [28][2]. We assume that the frequency regulation is instantaneous, but the voltage control happens with a delay that, following standard practice, is represented by a first order filter. Consequently, the inverter at the i–th node is represented by

$$\begin{aligned} \dot{\delta}_i &= u_i^{\delta}, \\ \tau_{V_i}\dot{V}_i &= -V_i + u_i^{\mathrm{V}}, \end{aligned} \tag{3}$$

where $u_i^{\delta} : \mathbb{R}_{\geq 0} \to \mathbb{R}$ and $u_i^{V} : \mathbb{R}_{\geq 0} \to \mathbb{R}$ are controls and $\tau_{V_i} \in \mathbb{R}_{>0}$ is the time constant of a low–pass filter.

Differently from SG units, inverters do not have an inherent physical relation between frequency and generated active power. Frequency droop control aims at artificially creating such a relation, since it is desired in many applications [10]. The rationale behind the droop controller is as follows [3, 15]. For small angular deviations δ_{ik} we have that $\sin(\delta_{ik}) \approx \delta_{ik}$ while $\cos(\delta_{ik}) \approx 1$. Hence, for dominantly inductive networks, *i.e.* $G_{ik} \approx 0$, from the

[1] To simplify notation the time argument of all signals is omitted.

[2] An underlying assumption to this model is that whenever the inverter connects an intermittent renewable generation source, *e.g.*, a photovoltaic plant or a wind plant, to the network, this is equipped with some sort of storage (*e.g.*, flywheel, battery). Thus, it can increase and decrease its power output within a certain range.

power equations (1) it is clear that the reactive power is mostly influenced by changes in the voltage, while the active power depends "more directly" on angular deviations. Consequently, the frequencies ω_i and voltage amplitudes V_i of the inverters are modified depending on the deviations (with respect to a desired value) of the active and reactive powers, respectively.

Simple proportional controllers are then implemented as

$$\begin{aligned} u_i^\delta &= \omega^d - k_{P_i}(P_i^m - P_i^d), \\ u_i^V &= V_i^d - k_{Q_i}(Q_i^m - Q_i^d), \end{aligned} \tag{4}$$

where $\omega^d \in \mathbb{R}_{>0}$ is the desired (nominal) frequency, $V_i^d \in \mathbb{R}_{>0}$ the desired (nominal) voltage amplitude, $k_{P_i} \in \mathbb{R}_{>0}$, respectively $k_{Q_i} \in \mathbb{R}_{>0}$, the frequency, respectively voltage, droop gain, $P_i^m : \mathbb{R}_{\geq 0} \to \mathbb{R}$ and $Q_i^m : \mathbb{R}_{\geq 0} \to \mathbb{R}$ are the measured powers and $P_i^d \in \mathbb{R}$ and $Q_i^d \in \mathbb{R}$ their desired setpoints. It is assumed that the powers are measured and processed through filters [4, 32], *i.e.*

$$\begin{aligned} \tau_{P_i}\dot{P}_i^m &= -P_i^m + P_i, \\ \tau_{P_i}\dot{Q}_i^m &= -Q_i^m + Q_i, \end{aligned} \tag{5}$$

where P_i and Q_i are given in (1) and $\tau_{P_i} \in \mathbb{R}_{>0}$ is the time constant of the low pass filters.

Note that the statements on small angular deviations δ_{ik} and small transfer conductances, *i.e.* $G_{ik} \approx 0$, are not an underlying assumption of the physical model given by (1), (3) and (5), but only serve to explain the physical and heuristic motivation behind the control laws (4).

Replacing (4) and (5) in (3) yields the closed–loop system

$$\begin{aligned} \dot{\delta}_i &= \omega^d - k_{P_i}(P_i^m - P_i^d), \\ \tau_{P_i}\dot{P}_i^m &= -P_i^m + P_i, \\ \tau_{V_i}\dot{V}_i &= -V_i + V_i^d - k_{Q_i}(Q_i^m - Q_i^d), \\ \tau_{P_i}\dot{Q}_i^m &= -Q_i^m + Q_i. \end{aligned} \tag{6}$$

In general $\tau_{V_i} \ll \tau_{P_i}$, hence we assume in the sequel $\tau_{V_i} = 0$. Setting $\tau_{V_i} = 0$ in (6) yields the algebraic equation $V_i = V_i^d - k_{Q_i}(Q_i^m - Q_i^d)$. Recall that $\dot{\delta}_i = \omega_i = \omega^d - k_{P_i}(P_i^m - P_i^d)$. Differentiating ω_i, respectively V_i, with respect to time gives $\dot{\omega}_i = -k_{P_i}\dot{P}_i^m$, respectively $\dot{V}_i = -k_{Q_i}\dot{Q}_i^m$. Using at first (6) to substitute $\dot{P}_i^m$, respectively $\dot{Q}_i^m$, and subsequently the indicated equations for ω_i, respectively V_i, to substitute P_i^m, respectively Q_i^m, finally yields

$$\begin{aligned} \dot{\delta}_i &= \omega_i, \\ \tau_{P_i}\dot{\omega}_i &= -\omega_i + \omega^d - k_{P_i}(P_i - P_i^d), \\ \tau_{P_i}\dot{V}_i &= -V_i + V_i^d - k_{Q_i}(Q_i - Q_i^d), \end{aligned} \tag{7}$$

where ω_i denotes the inverter frequency, see also [36]. To simplify notation we define

$$\begin{aligned} P^d &:= \mathrm{col}(P_i^d) \in \mathbb{R}^n,\ P := \mathrm{col}(P_i) \in \mathbb{R}^n, \\ Q^d &:= \mathrm{col}(Q_i^d) \in \mathbb{R}^n,\ Q := \mathrm{col}(Q_i) \in \mathbb{R}^n, \\ V^d &:= \mathrm{col}(V_i^d) \in \mathbb{R}^n,\ T := \mathrm{diag}(\tau_{P_i}) \in \mathbb{R}^{n\times n}, \\ K_P &:= \mathrm{diag}(k_{P_i}) \in \mathbb{R}^{n\times n},\ K_Q := \mathrm{diag}(k_{Q_i}) \in \mathbb{R}^{n\times n}, \end{aligned} \tag{8}$$

and write the system compactly as

$$\begin{aligned} \dot{\delta} &= \omega, \\ T\dot{\omega} &= -\omega + \mathbb{1}_n\omega^d - K_P(P - P^d), \\ T\dot{V} &= -V + V^d - K_Q(Q - Q^d), \end{aligned} \tag{9}$$

with power flows P and Q given in (1). We furthermore associate to each inverter its power rating $S_i^N \in \mathbb{R}_{>0}$, $i \sim \bar{n}$.

Remark 3.1. The desired power setpoints for active and reactive power P_i^d and Q_i^d, $i \sim \bar{n}$, are assumed to be transmitted to each inverter by a high–level control, *i.e.* typically a secondary control or energy management system.

Remark 3.2. Since an inverter may connect a pure storage device, *e.g.*, a battery, to the network, P_i^d can also take negative values. In that case, the storage device is charged depending on the excess power available in the network and thus functions as a frequency and voltage dependent load. In the sequel, we refer to such an operation mode as charging mode.

Remark 3.3. In [36] it is proven that the dynamics of an inverter with frequency droop control and the swing equation dynamics of an SG are equivalent. Consequently, an inverter operated in voltage source mode and with frequency droop achieves a behavior similar to that of an SG with respect to frequency, which is desired in many microgrid applications [10, 25].

Remark 3.4. There are several other alternative droop control schemes proposed in the literature, *e.g.,* [43, 16, 15]. The one given in (4) is the most common one for dominantly inductive networks, as well as the one most compatible with the operation of conventional power systems [10]. We therefore restrict our analysis to these control laws, commonly referred to as "conventional droop control".

4. Boundedness of trajectories

The proposition below gives conditions for global boundedness of the trajectories of the system (9), (1), which we recall lives in the set

$$\mathbb{M} := \mathbb{S}^n \times \mathbb{R}^n \times \mathbb{R}^n_{>0}. \tag{10}$$

To establish our result, we need the following assumption on the network susceptances that particularly holds for dominantly inductive networks. The droop controls (4) are predominantly employed in such networks.

Assumption 4.1.

$$\hat{B}_{ii} \leq 0 \text{ and } B_{ik} \leq 0,\ i \sim \bar{n},\ k \sim \bar{n}. \tag{11}$$

Proposition 4.2. *Consider the system* (9), (1) *with Assumption 4.1. The set* $\mathbb{M}$ *defined in* (10) *is invariant and all trajectories of* (9), (1) *are bounded if* V_i^d, k_{Q_i} *and* Q_i^d *are chosen such that*

$$V_i^d + k_{Q_i} Q_i^d > 0, \quad i \sim \bar{n}. \tag{12}$$

Proof. From (7), (1), write $\tau_{P_i}\dot{V}_i = f_{3i}(\delta, V)$, for some function $f_{3i} : \mathbb{S}^n \times \mathbb{R}^n_{>0} \to \mathbb{R}$. Note that

$$f_{3i}(V,\delta)_{|V_i=0} = V_i^d + k_{Q_i} Q_i^d,$$

which, under condition (12), is positive. Hence, the following implication is true

$$V_i(0) > 0 \ \Rightarrow\ V_i(t) > 0,$$

for all $t \geq 0$. This proves that the set $\mathbb{M}$ is invariant.

To establish boundedness of solutions define the matrix $\Gamma := \mathrm{diag}(\tau_{P_i}/k_{Q_i})$, $i \sim \bar{n}$ and the function $W : \mathbb{R}^n \to \mathbb{R}_{>0}$

$$W(V) = \|\Gamma V\|_1 = \sum_{i=1}^{n} \frac{\tau_{P_i}}{k_{Q_i}} V_i,$$

with $\|\cdot\|_1$ the 1–norm. Then,

$$\begin{aligned} \dot{W} &= \sum_{i=1}^{n} \left(\frac{1}{k_{Q_i}}(-V_i + V_i^d) - (Q_i(\delta, V) - Q_i^d) \right) \\ &\leq -\kappa_1 W + \kappa_2 - V^\top \mathcal{T}(\delta) V, \end{aligned}$$

where

$$\kappa_1 := \min_{i \in \bar{n}} \left\{ \frac{1}{\tau_{P_i}} \right\}, \quad \kappa_2 := \sum_{i=1}^{n} \left(\frac{1}{k_{Q_i}} V_i^d + Q_i^d \right)$$

and $\mathcal{T} : \mathbb{S}^n \to \mathbb{R}^{n \times n}$ with

$$\begin{aligned} (\mathcal{T}(\delta))_{ii} &:= -B_{ii}, \\ (\mathcal{T}(\delta))_{ik} &:= B_{ik} \cos(\delta_{ik}),\ i \neq k. \end{aligned} \tag{13}$$

Here, we have used the fact that, as $G_{ik} = G_{ki}$, (1) implies that

$$\sum_{i=1}^{n} Q_i = \sum_{i=1}^{n} \left(-B_{ii} V_i^2 + \sum_{k \sim \mathcal{N}_i} B_{ik} V_i V_k \cos(\delta_{ik}) \right),$$

which are the reactive power losses in the network.

Since $B_{ik} = B_{ki}$, $\mathcal{T}(\delta)$ is symmetric and (2) together with (11) implies that

$$\mathcal{T}(\delta) \geq n \kappa_3 \Gamma^2,$$

for some $\kappa_3 \geq 0$. Hence

$$\dot{W} \leq -\kappa_1 W + \kappa_2 - \kappa_3 W^2,$$

where the third right hand term follows from

$$n V^\top \Gamma^2 V \geq \|\Gamma V\|_1^2 = W^2(V).$$

Assume $\kappa_3 > 0$. The differential equation

$$\dot{z} = -\kappa_1 z + \kappa_2 - \kappa_3 z^2, \quad z(0) = z_0,$$

is a scalar differential Riccati equation with constant coefficients, which has the solution

$$z(t) = \frac{2\kappa_2 \left(-1 + e^{\kappa_4 t}\right) + z_0 \left(\kappa_1 \left(1 - e^{\kappa_4 t}\right) + \kappa_4 \left(1 + e^{\kappa_4 t}\right)\right)}{\kappa_1 \left(-1 + e^{\kappa_4 t}\right) + \kappa_4 \left(1 + e^{\kappa_4 t}\right) + 2\kappa_3 z_0 \left(-1 + e^{\kappa_4 t}\right)}, \tag{14}$$

with $\kappa_4 := \sqrt{4\kappa_2\kappa_3 + \kappa_1^2}$. Furthermore,

$$\lim_{t \to \infty} z(t) = \frac{2\kappa_2 + z_0 \left(-\kappa_1 + \kappa_4\right)}{\kappa_1 + \kappa_4 + 2\kappa_3 z_0}. \tag{15}$$

From the Comparison Lemma [22] we then have for $W(V(0)) \leq z_0$

$$\sum_{i=1}^{n} \frac{\tau_{P_i}}{k_{Q_i}} V_i(t) \leq z(t),$$

hence, together with (15), $V \in \mathcal{L}_\infty$. This, together with (1), implies that $P \in \mathcal{L}_\infty$. Finally, $\omega \in \mathcal{L}_\infty$ follows from (7), which shows that ω_i is the output of a linear time invariant (LTI) asymptotically stable system with bounded input.

If $\kappa_3 = 0$ we have $\dot{W} \leq -\kappa_1 W + \kappa_2$, and the proof follows immediately. □□□

Remark 4.3. Condition (12) in Proposition 4.2 has a clear physical interpretation. From the dynamics of V_i in (7) we see that the equilibrium voltage is given by

$$V_i^s = V_i^d - k_{Q_i}(Q_i^s - Q_i^d),$$

where Q_i^s is the reactive power injected in steady–state to the i–th bus. Hence, (12) requires that the gains k_{Q_i} and the setpoints V_i^d and Q_i^d of the voltage droop control (4) are chosen such that $V_i^s > 0$, even if there is zero reactive power injection to the i–th bus. Notice that condition (12) is satisfied for all k_{Q_i} if $Q_i^d \geq 0$.

5. Stability for lossless microgrids

In this section we derive conditions for stability for *lossless microgrids*, *i.e.* $G_{ik} = 0, i \sim \bar{n}, k \sim \bar{n}$. The assumption of lossless line admittances may be justified as follows: in MV and LV networks the line impedance is usually not purely inductive, but has a non–negligible resistive part. On the other hand, the inverter output impedance is typically inductive (due to the output inductance and/or the possible presence of an output transformer). Under these circumstances, the inductive parts dominate the resistive parts.

We only consider such microgrids and absorb the inverter output admittance (together with the possible transformer admittance), $\tilde{Y}_{ik}$, into the line admittances, Y_{ik},

while neglecting all resistive effects. This assumption is further justified for the present analysis, since the droop control laws introduced in (4) are mostly used in networks with dominantly inductive admittances [16, 15].

Therefore, we make the following assumption on the network admittances.

Assumption 5.1. *$G_{ik}=0$ and $B_{ik}\leq 0,\ i\sim\bar{n},\ k\sim\bar{n}$.*

By making use of Assumption 5.1, the power flow equations (1) for a lossless microgrid reduce to

$$\begin{aligned} P_i &= \sum_{k\sim\mathcal{N}_i} |B_{ik}|V_iV_k\sin(\delta_{ik}),\\ Q_i &= |B_{ii}|V_i^2 - \sum_{k\sim\mathcal{N}_i} |B_{ik}|V_iV_k\cos(\delta_{ik}). \end{aligned}$$

Remark 5.2. The need to introduce the, sometimes unrealistic, assumption of lossless admittances has a long history in power systems studies. It appears in transient stability studies, where the presence of transfer conductances hampers the derivation of energy–Lyapunov functions [41]. Although there has been progress in addressing this issue [2, 9], to the best of our knowledge no analytic solution for power systems with variable frequencies as well as variable voltage amplitudes is available. See also [29] for an illustration of the deleterious effect of line losses on field excitation controller design.

Remark 5.3. In the case of the Kron–reduced network, we are aware that, in general, the reduced network admittance matrix does not permit to neglect the conductances and our stability results might therefore be inaccurate [41]. Alternatively, one could consider the idealized scenario in which part of the inverter–interfaced storage devices are being charged, hence acting as loads and all constant impedance loads are neglected. Another approach is to use other, possibly dynamic, load models instead of constant impedances in the so–called structure preserving power system models. However, in the presence of variable voltages the load models are usually, somehow artificially, adapted to fit the theoretical framework used for the construction of energy–Lyapunov functions, see *e.g.,* [5, 14].

5.1. Synchronized motion

To state the main result of this section we need the following natural power–balance feasibility assumption.

Assumption 5.4. *There exist constants $\delta^s\in\Theta$, $\omega^s\in\mathbb{R}$ and $V^s\in\mathbb{R}^n_{>0}$, where*

$$\Theta := \left\{\delta\in\mathbb{S}^n \;\middle|\; |\delta_{ik}|<\frac{\pi}{2}, i\sim\bar{n},\ k\sim\mathcal{N}_i\right\},$$

such that

$$\begin{aligned} \mathbb{1}_n\omega^s - \mathbb{1}_n\omega^d + K_P[P(\delta^s,V^s)-P^d] &= \underline{0}_n,\\ V^s - V^d + K_Q[Q(\delta^s,V^s)-Q^d] &= \underline{0}_n. \end{aligned} \tag{16}$$

Under Assumption 5.4, the motion of the system (9), (1) starting in $(\delta^s,\mathbb{1}_n\omega^s,V^s)$ is given by

$$\begin{aligned} \delta^*(t) &= \mathrm{mod}_{2\pi}\{\delta^s+\mathbb{1}_n\omega^s t\},\\ \omega^*(t) &= \mathbb{1}_n\omega^s,\\ V^*(t) &= V^s, \end{aligned} \tag{17}$$

where the operator[3] $\mathrm{mod}_{2\pi}\{\cdot\}$ is added to respect the topology of the system. This desired motion is called synchronized motion and ω^s is the synchronization frequency.

Remark 5.5. As done in [38], where a similar analysis is made for lossless networks with first–order inverter dynamics, it is possible to uniquely determine ω^s. Towards this end, recall the well–known fact that in a lossless power system

$$\sum_{i\sim\bar{n}} P_i^s = 0.$$

Thus, replacing the synchronized motion (17) in (7) and adding up all the nodes yields

$$\sum_{i\sim\bar{n}}\frac{\dot{\omega}_i}{k_{P_i}} = 0 \quad\Rightarrow\quad \omega^s = \omega^d + \frac{\sum\limits_{i\sim\bar{n}} P_i^d}{\sum\limits_{i\sim\bar{n}}\frac{1}{k_{P_i}}}.$$

It follows that $i\sim\bar{n}$

$$\begin{aligned} &\frac{1}{k_{P_i}}(\omega^s-\omega^d) - P_i^d = \sum_{k\sim\bar{n},k\neq i}\left(\frac{1}{k_{P_k}}(\omega^d-\omega^s)+P_k^d\right)\\ &\Leftrightarrow \omega^s-\omega^d-k_{P_i}P_i^d = \sum_{k\sim\bar{n},k\neq i}\frac{k_{P_i}}{k_{P_k}}\left(\omega^d-\omega^s+k_{P_k}P_k^d\right). \end{aligned} \tag{18}$$

Remark 5.6. Clearly, the synchronized motion lives in the set $\Theta\times\mathbb{1}_n\omega^s\times\mathbb{R}^n_{>0}$.

Remark 5.7. There is not a unique desired synchronized motion of the system (9), (1) associated to the flow given in (16), but any motion with $\omega^*(t)$ and $V^*(t)$ as given in (17) and $\delta^*(t)=\mathrm{mod}_{2\pi}\{\delta^s+\mathbb{1}_n\omega^s t+\alpha\mathbb{1}_n\}$, $\alpha\in\mathbb{R}$ is a desired synchronized motion.

5.2. Error dynamics

The main result of this section is to give conditions on the setpoints and gains of the droop controller (4) such that the synchronized motion (17) is asymptotically stable, *i.e.* such that all trajectories of the system (9), (1) converge to the synchronized motion (17) (up to a uniform shift of all angles). To establish this result we make the important observation that the dependence with respect to δ of the dynamics (9), (1) is via angle differences

[3] The operator $\mathrm{mod}_{2\pi}\{\cdot\}:\mathbb{R}\to[0,2\pi)$, is defined as follows: $y=\mathrm{mod}_{2\pi}\{x\}$ yields $y=x-k2\pi$ for some integer k with $\mathrm{sign}(y)=\mathrm{sign}(x)$ and $y\in[0,2\pi)$.

δ_{ik}. This immediately leads to the following two implications: *(i)* the flow given in (16) is invariant to a shift in the δ coordinate of the form $\delta + \mathbb{1}_n \omega^s t$. Consequently, we can study the stability of the synchronized motion (17) in the coordinates $\mathrm{col}(\tilde{\delta}(t), \tilde{\omega}(t), V(t)) \in \mathbb{R}^n \times \mathbb{R}^n \times \mathbb{R}^n_{>0}$ with

$$\begin{aligned} \tilde{\omega}(t) &:= \omega(t) - \mathbb{1}_n \omega^s, \\ \tilde{\delta}(t) &:= \delta(0) + \int_0^t \tilde{\omega}(\tau) d\tau, \end{aligned}$$

where – for convenience – we have also shifted the coordinate ω; *(ii)* convergence of the dynamics (9), (1) to the desired synchronized motion (17) (up to a uniform shift of all angles) is not determined by the value of the angles, but only by their differences. Hence, to study convergence to the synchronized motion (17) we can arbitrarily choose one node, say node n, as a reference node and express $\tilde{\delta}_i$ for all $i \in \bar{n} \backslash \{n\}$ relative to $\tilde{\delta}_n$ via the state transformation

$$\theta := \mathcal{R}\tilde{\delta}, \quad \mathcal{R} := \begin{bmatrix} I_{(n-1)} & -\mathbb{1}_{(n-1)} \end{bmatrix}. \tag{19}$$

This leads to a reduced system of order $3n-1$ with $\theta = \mathrm{col}(\theta_1, \ldots, \theta_{n-1})$ replacing $\tilde{\delta}$. For convenience, we define the *constant*[4]

$$\theta_n := 0,$$

as well as

$$\theta_{ik} := \theta_i - \theta_k,$$

which clearly verifies $\theta_{ik} \equiv \delta_{ik}$ for $k \neq n$ and $\theta_{in} \equiv \theta_i$.

Furthermore, we introduce the constants

$$c_{1_i} := \omega^d - \omega^s + k_{P_i} P_i^d, \; c_{2_i} := V_i^d + k_{Q_i} Q_i^d, \; i \sim \bar{n}. \tag{20}$$

Written in the new coordinates $\mathrm{col}(\theta, \tilde{\omega}, V) \in \mathbb{R}^{n-1} \times \mathbb{R}^n \times \mathbb{R}^n_{>0}$ the dynamics (9), (1) take the form

$$\begin{aligned} \dot{\theta}_i &= \tilde{\omega}_i - \tilde{\omega}_n, \\ \tau_{P_i} \dot{\tilde{\omega}}_i &= -\tilde{\omega}_i - k_{P_i} \sum_{k \sim \mathcal{N}_i} V_i V_k |B_{ik}| \sin(\theta_{ik}) + c_{1_i}, \\ \tau_{P_i} \dot{V}_i &= -V_i - k_{Q_i} \big(|B_{ii}| V_i^2 - \sum_{k \sim \mathcal{N}_i} V_i V_k |B_{ik}| \cos(\theta_{ik}) \big) + c_{2_i}, \end{aligned} \tag{21}$$

for all $i \in \bar{n} \setminus \{n\}$. The dynamics of the n–th node, which serves as a reference, are given by

$$\begin{aligned} \tau_{P_n} \dot{\tilde{\omega}}_n &= -\tilde{\omega}_n + k_{P_n} \sum_{k \sim \mathcal{N}_n} V_n V_k |B_{nk}| \sin(\theta_k) + c_{1_n}, \\ \tau_{P_n} \dot{V}_n &= -V_n - k_{Q_n} \big(|B_{nn}| V_n^2 - \sum_{k \sim \mathcal{N}_n} V_n V_k |B_{nk}| \cos(\theta_k) \big) + c_{2_n}. \end{aligned} \tag{22}$$

The reduced system (21)–(22) lives in the set $\tilde{\mathbb{M}} = \mathbb{R}^{n-1} \times \mathbb{R}^n \times \mathbb{R}^n_{>0}$. Note that this system has an equilibrium at

$$x^s := \mathrm{col}(\theta^s, \underline{0}_n, V^s), \tag{23}$$

the asymptotic stability of which implies asymptotic convergence of all trajectories of the system (9), (1) to the synchronized motion (17) up to a uniform shift of all angles.

[4]The constant θ_n is not part of the state vector θ.

5.3. Main result

To streamline the presentation of the stability result we introduce the matrices $\mathcal{L} \in \mathbb{R}^{(n-1)\times(n-1)}$ and $\mathcal{W} \in \mathbb{R}^{(n-1)\times n}$ with entries

$$\begin{aligned} l_{ii} &:= \sum_{m=1}^n |B_{im}| V_i^s V_m^s \cos(\theta_{im}^s), \, l_{ik} := -|B_{ik}| V_i^s V_k^s \cos(\theta_{ik}^s), \\ w_{ii} &:= \sum_{m=1}^n |B_{im}| V_m^s \sin(\theta_{im}^s), \, w_{im} := |B_{im}| V_i^s \sin(\theta_{im}^s), \end{aligned} \tag{24}$$

where $i \sim \bar{n} \setminus \{n\}$, $k \sim \bar{n} \setminus \{n\}$ and $m \sim \bar{n}$, as well as

$$\mathcal{D} := \mathrm{diag}\left(\frac{c_{2_m}}{k_{Q_m} (V_m^s)^2} \right) = \mathrm{diag}\left(\frac{V_m^d + k_{Q_m} Q_m^d}{k_{Q_m} (V_m^s)^2} \right) \in \mathbb{R}^{n \times n}. \tag{25}$$

We also recall the matrix $\mathcal{T}$ defined in (13) and, with slight abuse of notation, denote by $\mathcal{T}(\theta^s)$ its evaluation at $\theta^s \in \mathbb{R}^{n-1}$ with entries

$$t_{ii} = |B_{ii}|, \quad t_{ik} = -|B_{ik}| \cos(\theta_{ik}^s), \; i \neq k, \; i \sim \bar{n}, \; k \sim \bar{n}.$$

From (2), and under Assumption 5.1, it follows that $\mathcal{T}(\theta^s)$ is positive semidefinite.

Lemma 5.8. *Consider the system* (9), (1) *with Assumptions 5.1 and 5.4. Then* $\mathcal{L} > 0$.

Proof. Consider the vector P defined in (8) under Assumption 5.1 and let $\tilde{L}$ be given by

$$\tilde{L} := \frac{\partial P}{\partial \delta}\Big|_{(\delta^s, V^s)} \in \mathbb{R}^{n \times n}, \tag{26}$$

with entries

$$\tilde{l}_{ii} := \sum_{k \sim \mathcal{N}_i} |B_{ik}| V_i^s V_k^s \cos(\delta_{ik}^s), \; \tilde{l}_{ik} := -|B_{ik}| V_i^s V_k^s \cos(\delta_{ik}^s).$$

Clearly, from (24), $\tilde{l}_{ii} = l_{ii}$ and $\tilde{l}_{ik} = l_{ik}$ for $k \neq n$. Furthermore, recall that the microgrid is connected by assumption. It is easily verified that under the given assumptions $\tilde{L}$ is a symmetric Laplacian matrix of a connected graph with the properties [13], see also *e.g.,* [38, 36],

$$\tilde{L} \gamma \mathbb{1}_n = 0, \; v^\top \tilde{L} v > 0, \; \forall v \in \mathbb{R}^n \setminus \{v = \gamma \mathbb{1}_n\}, \; \gamma \in \mathbb{R}. \tag{27}$$

Recall the matrix $\mathcal{R}$ defined in (19), let $r := \begin{bmatrix} \underline{0}_{(n-1)}^\top & 1 \end{bmatrix}$ and note that

$$\tilde{L} \begin{bmatrix} \mathcal{R} \\ r \end{bmatrix}^{-1} = \tilde{L} \begin{bmatrix} I_{(n-1)} & \mathbb{1}_{(n-1)} \\ \underline{0}_{(n-1)}^\top & 1 \end{bmatrix} = \begin{bmatrix} \mathcal{L} & \underline{0}_{n-1} \\ b^\top & 0 \end{bmatrix}, \tag{28}$$

where $b = \mathrm{col}(\tilde{l}_{in}) \in \mathbb{R}^{(n-1)}$, $i \sim \bar{n} \setminus \{n\}$. It follows from (27) and (28) that for any $\tilde{v} := \mathrm{col}(\vartheta, 0) \in \mathbb{R}^n$, $\vartheta \in \mathbb{R}^{(n-1)}$

$$\tilde{v}^\top \tilde{L} \begin{bmatrix} \mathcal{R} \\ r \end{bmatrix}^{-1} \tilde{v} = \tilde{v}^\top \tilde{L} \tilde{v} = \vartheta^\top \mathcal{L} \vartheta > 0. \tag{29}$$

Moreover, $\mathcal{L}$ is symmetric. Hence, $\mathcal{L} > 0$. □□□

It follows from (29) and the properties of spectra of symmetric matrices, see *e.g.* [20], that, under the standing assumptions of Lemma 5.8,

$$\sigma(\mathcal{L}) \subseteq \sigma(\tilde{L}) \setminus \{0\} \subset \mathbb{R}_{>0}, \tag{30}$$

with $\tilde{L}$ given in (26). Notice that the matrices $\mathcal{L}$, respectively $\tilde{L}$, correspond to the linearization of the active power flows at nodes $i \sim \bar{n}\setminus\{n\}$ in the reduced system (21)–(22), respectively to the linearization of the active power flows at all nodes $i \sim \bar{n}$ in the original system (9), (1). Hence, $\mathcal{L}$, respectively $\tilde{L}$, represent locally the network coupling strengths between the phase angles and the active power flows. Consequently, (30) states that the local coupling strengths between the phase angles and the active power flows in the reduced system (21)–(22) are contained within the local coupling strengths between the phase angles and the active power flows in the original system (9), (1).

We are now ready to state our main result.

Proposition 5.9. *Consider the system* (9), (1) *with Assumptions 5.1 and 5.4. Fix* τ_{P_i}, k_{P_i} *and* P_i^d, $i \sim \bar{n}$. *Select* V_i^d, k_{Q_i} *and* Q_i^d *such that*

$$\mathcal{D} + \mathcal{T}(\theta^s) - \mathcal{W}^\top \mathcal{L}^{-1} \mathcal{W} > 0. \tag{31}$$

Then the equilibrium $x^s = col(\theta^s, \underline{0}_n, V^s)$ *of the system* (21)–(22) *is locally asymptotically stable.*

Proof. To establish the claim we follow the interconnection and damping assignment passivity–based control approach [30], and represent the system (21)–(22) in port–Hamiltonian form to identify the energy–Lyapunov function. Defining $x := \mathrm{col}(\theta, \tilde{\omega}, V)$, we can write the system (21)–(22) as

$$\dot{x} = (J - R(x))\nabla H, \tag{32}$$

where the Hamiltonian $H : \mathbb{R}^{(n-1)} \times \mathbb{R}^n \times \mathbb{R}^n_{>0} \to \mathbb{R}$ is given by

$$\begin{aligned} H(x) = &\sum_{i=1}^{n} \Big(\frac{\tau_{P_i}}{2k_{P_i}} \tilde{\omega}_i^2 + \frac{1}{k_{Q_i}}(V_i - c_{2_i} \ln(V_i)) + \frac{1}{2}|B_{ii}|V_i^2 \\ &- \frac{1}{2} \sum_{k \sim \mathcal{N}_i} V_i V_k |B_{ik}| \cos(\theta_{ik}) \Big) - \sum_{i=1}^{n-1} \frac{c_{1i}}{k_{P_i}} \theta_i \end{aligned} \tag{33}$$

and the interconnection and damping matrices are

$$J = \begin{bmatrix} 0_{(n-1)\times(n-1)} & \mathcal{J} \\ -\mathcal{J}^\top & 0_{2n\times 2n} \end{bmatrix}, R = \mathrm{diag}(\underline{0}_{(n-1)}, R_\omega, R_V) \tag{34}$$

with $\mathcal{J} = \begin{bmatrix} \mathcal{J}_K & -\frac{k_{P_n}}{\tau_{P_n}} \mathbb{1}_{(n-1)} & 0_{(n-1)\times n} \end{bmatrix}$,

$$\mathcal{J}_K = \mathrm{diag}\left(\frac{k_{P_k}}{\tau_{P_k}} \right) \in \mathbb{R}^{(n-1)\times(n-1)},\ k \sim \bar{n} \setminus \{n\},$$

$$R_\omega = \mathrm{col}\left(\frac{k_{P_i}}{\tau_{P_i}^2} \right) \in \mathbb{R}^n,\ R_V = \mathrm{col}\left(\frac{k_{Q_i} V_i}{\tau_{P_i}} \right) \in \mathbb{R}^n,$$

$i \sim \bar{n}$. Note that $J = -J^\top$ and $R \geq 0$. Consequently,

$$\dot{H} = -(\nabla H)^\top R \nabla H \leq 0. \tag{35}$$

Therefore, x^s is a stable equilibrium of system (21)–(22) if $H(x)$ has a strict local minimum at the equilibrium x^s. To ensure the latter we show that $\nabla H(x^s) = \underline{0}_{(3n-1)}$ and $\frac{\partial^2 H(x)}{\partial x^2}\big|_{x^s} > 0$. Now,

$$\left(\frac{\partial H}{\partial \theta}\Big|_{x^s} \right)^\top = \mathrm{col}\big(a_i - \frac{c_{1_i}}{k_{P_i}}\big) \in \mathbb{R}^{(n-1)}, \quad \left(\frac{\partial H}{\partial \tilde{\omega}}\Big|_{x^s} \right)^\top = \underline{0}_n,$$

$$\left(\frac{\partial H}{\partial V}\Big|_{x^s} \right)^\top = \mathrm{col}\left(-b_l + |B_{ll}|V_l^s + \frac{1}{k_{Q_l}} \left(1 - \frac{c_{2_l}}{V_l^s} \right) \right) \in \mathbb{R}^n,$$

where $i \sim \bar{n} \setminus \{n\}$, $l \sim \bar{n}$ and

$$a_i := \sum_{k \sim \mathcal{N}_i} V_i^s V_k^s |B_{ik}| \sin(\theta_{ik}^s),\ b_l := \sum_{k \sim \mathcal{N}_l} V_k^s |B_{lk}| \cos(\theta_{lk}^s).$$

Hence, $\nabla H(x^s) = \underline{0}_{(3n-1)}$.

The Hessian of $H(x)$ evaluated at x^s is given by

$$\frac{\partial^2 H(x)}{\partial x^2}\Big|_{x^s} = \begin{bmatrix} \mathcal{L} & 0_{(n-1)\times n} & \mathcal{W} \\ 0_{n\times(n-1)} & \mathcal{A} & 0_{n\times n} \\ \mathcal{W}^\top & 0_{n\times n} & \mathcal{D} + \mathcal{T}(\theta^s) \end{bmatrix},$$

with $\mathcal{L}$, $\mathcal{W}$, $\mathcal{D}$ and $\mathcal{T}(\theta^s)$ as defined in (24), (25), respectively (13), and $\mathcal{A} := \mathrm{diag}(\tau_{P_i}/k_{P_i}) \in \mathbb{R}^{n\times n}$. Since $\mathcal{A}$ is positive definite, the Hessian is positive definite if and only if the submatrix

$$\begin{bmatrix} \mathcal{L} & \mathcal{W} \\ \mathcal{W}^\top & \mathcal{D} + \mathcal{T}(\theta^s) \end{bmatrix} \tag{36}$$

is positive definite. Recall that Lemma 5.8 implies that, under the standing assumptions, $\mathcal{L}$ is positive definite. Hence, the matrix (36) is positive definite if and only if

$$\mathcal{D} + \mathcal{T}(\theta^s) - \mathcal{W}^\top \mathcal{L}^{-1} \mathcal{W} > 0,$$

which is condition (31).

Recalling (35) and the fact that $R(x) \geq 0$, we see that to prove asymptotic stability it suffices to show that – along the trajectories of the system (32) – the implication

$$R(x(t))\nabla H(x(t)) \equiv \underline{0}_{(3n-1)} \ \Rightarrow \lim_{t\to\infty} x(t) = x^s \tag{37}$$

holds. From (37) it follows that

$$\frac{\partial H}{\partial \tilde{\omega}} = \underline{0}_n,\ \frac{\partial H}{\partial V} = \underline{0}_n,$$

where the first condition implies $\tilde{\omega} = \underline{0}_n$. Hence, θ is constant. The second condition implies V constant. Therefore, the invariant set where $\dot{H}(x(t)) \equiv 0$ is an equilibrium. To prove that this is the desired equilibrium x^s we recall that x^s is an isolated minimum of $H(x)$. Consequently, there is a neighborhood of x^s where no other equilibrium exists, completing the proof. □□□

Condition (31) has the following physical interpretation: the droop control laws (4) establish a feedback interconnection linking the phase angles δ, respectively θ, with the active power flows P, as well as the voltages V with the reactive power flows Q.

The matrices $\mathcal{L}$ and $\mathcal{T}(\theta^s)$ represent then the network coupling strengths between the phase angles and the active power flows, respectively, the voltages and the reactive power flows. In the same way, $\mathcal{W}$ can be interpreted as a local cross–coupling strength originating from the fact that $P \neq P(\delta)$ and $Q \neq Q(V)$, but $P = P(\delta, V)$ and $Q = Q(\delta, V)$.

Condition (31) states that to ensure local stability of the equilibrium x^s defined in (23) the couplings represented by $\mathcal{L}$ and $\mathcal{T}(\theta^s)$ have to dominate over the cross–couplings of the power flows contained in $\mathcal{W}$. If that is not the case the voltage variations have to be reduced by reducing the magnitudes of the gains k_{Q_i}, $i \in \bar{n}$.

Another possibility is to adapt Q_i^d and V_i^d. This does, however, not seem as appropriate in practice since these two parameters are typically setpoints provided by a high–level control, which depend on the nominal voltage of the network and the expected loading conditions, see Remark 3.1.

Remark 5.10. To see that (32) is indeed an equivalent representation of (21)–(22), note that the part of the dynamics of $\tilde{\omega}_n$ in (22) resulting from $J\nabla H$ is

$$\begin{aligned}\frac{k_{P_n}}{\tau_{P_n}}\mathbb{1}_{(n-1)}^\top \left(\frac{\partial H}{\partial \theta}\right)^\top &= \\ &= \frac{k_{P_n}}{\tau_{P_n}} \sum_{i=1}^{n-1} \Big(\sum_{k\sim\mathcal{N}_i} V_i V_k |B_{ik}| \sin(\theta_{ik}) - \frac{c_{1_i}}{k_{P_i}} \Big) \\ &= \frac{k_{P_n}}{\tau_{P_n}} \Big(\sum_{k\sim\mathcal{N}_n} V_n V_k |B_{nk}| \sin(\theta_k) - \sum_{i=1}^{n-1} \frac{c_{1_i}}{k_{P_i}} \Big),\end{aligned}$$

since $\sum_{i=1}^{n-1} \sum_{k\sim\mathcal{N}_i, k\neq n} V_i V_k |B_{ik}| \sin(\theta_{ik}) = 0$. Furthermore, it follows from (18) that

$$c_{1_n} = \omega^d - \omega^s + k_{P_n} P_n^d = -\sum_{i=1}^{n-1} \frac{k_{P_n}}{k_{P_i}} c_{1_i}.$$

Finally, the remaining term in $\tilde{\omega}_n$ is contributed by the dissipation part $R\nabla H$.

Remark 5.11. The analysis reveals that the stability properties of the lossless microgrid (9), (1) are independent of the frequency droop gains k_{P_i}, the active power setpoints P_i^d and the low pass filter time constants τ_{P_i}, and only condition (31) is imposed on V_i^d, k_{Q_i} and Q_i^d. In that regard, the result is identical to those derived for lossless first–order inverter models in [38] and lossless second–order inverter models in [36], both assuming constant voltage amplitudes.

5.4. A relaxed stability condition

Condition (31) is imposed to ensure $H(x)$ given in (33) is a positive definite function and, therefore, qualifies as a Lyapunov function candidate. This condition can be removed if, instead of Lyapunov theory, LaSalle's invariance principle (which does not require positive definiteness) is invoked [22]. Indeed, from the proof of Proposition 5.9 we have that the function $H(x)$ is still non–increasing and via LaSalle we can conclude that all *bounded* trajectories converge to an equilibrium.

The qualifier "bounded" is, of course, critical, and its establishment is stymied by the presence of the linear term in θ contained in $H(x)$ given in (33). The inclusion of this term destroys the natural topology of the system, *e.g.*, with $\theta \in \mathbb{S}^{n-1}$, and we have to look at the system with θ evolving in $\mathbb{R}^{n-1}$ – which is not a bounded set. See Remark 7 of [8] for further discussion on this point that, unfortunately, is often overlooked in the literature.

Fortunately, due to the structure of the system, there is a particular choice of the controller gains that allows us to remove this disturbing term, still preserving a port–Hamiltonian structure. As indicated in Remark 6.5, it turns out that this choice of gains is of interest because it guarantees the desired steady–state active power sharing.

The discussion above is formalized in the following corollary of Proposition 5.9.

Corollary 5.12. *Consider the system* (9), (1) *with Assumption 5.1. Fix* τ_{P_i}, k_{Q_i} *and* Q_i^d, $i \sim \bar{n}$. *Select*

$$k_{P_i} P_i^d = \xi, \tag{38}$$

$i \sim \bar{n}$ *and some real constant* ξ. *Then all trajectories of the system* (21)–(22) *converge to an equilibrium.*

Proof. Under condition (38), it follows from Remark 5.5 that

$$\omega^s = \omega^d + \frac{\sum_{i\sim\bar{n}} P_i^d}{\sum_{i\sim\bar{n}} \frac{1}{k_{P_i}}} = \omega^d + \frac{\xi \sum_{i\sim\bar{n}} \frac{1}{k_{P_i}}}{\sum_{i\sim\bar{n}} \frac{1}{k_{P_i}}} = \omega^d + \xi$$

and hence from (20) that $c_{1_i} = 0$ for all $i \in \bar{n}$. Consequently, it is possible to define the state $z := \mathrm{col}(\theta, \tilde{\omega}, V)$ in the set $\Gamma : \mathbb{S}^{n-1} \times \mathbb{R}^n \times \mathbb{R}^n_{>0}$ and represent the system (21)–(22) in port–Hamiltonian form as

$$\dot{z} = (J - R(z))\nabla\mathcal{H},$$

with Hamiltonian $\mathcal{H} : \mathbb{S}^{(n-1)} \times \mathbb{R}^n \times \mathbb{R}^n_{>0} \to \mathbb{R}$ given by

$$\begin{aligned}\mathcal{H}(z) = \sum_{i=1}^{n} \Big(&\frac{\tau_{P_i}}{2k_{P_i}} \tilde{\omega}_i^2 + \frac{1}{k_{Q_i}} (V_i - c_{2_i} \ln(V_i)) + \frac{1}{2} |B_{ii}| V_i^2 \\ &- \frac{1}{2} \sum_{k\sim\mathcal{N}_i} V_i V_k |B_{ik}| \cos(\theta_{ik}) \Big)\end{aligned} \tag{39}$$

and matrices J and R as defined in (34). Similarly to (35) we have that

$$\dot{\mathcal{H}} = -(\nabla\mathcal{H})^\top R \nabla\mathcal{H} \leq 0$$

and in analogy to (37) it holds that the invariant set where $\dot{H}(z(t)) \equiv 0$ is an equilibrium set. Moreover, it follows

from Proposition 4.2 that the state $z = \mathrm{col}(\theta, \tilde{\omega}, V) \in \Gamma$ is globally bounded. Hence, by LaSalle's invariance principle [22] all trajectories of the system (21)–(22) converge to an equilibrium. □□□

Note, however, that the claim critically relies on the fragile assumption that $c_{1i} = 0$ for all $i \in \bar{n}$. In the presence of small perturbations or model uncertainties, such as, for example, the presence of small conductances, the synchronization frequency is given by $\omega^s = \omega^d + \xi + \epsilon$, where ϵ is some small real nonzero constant. In that case $c_{1i} \neq 0$ under condition (38) and the proof of Corollary 5.12 is not applicable. Moreover, as usual in LaSalle's–based analysis, the absence of a *bona fide* Lyapunov function hampers the possibility of invoking a continuity argument to accommodate small disturbances.

6. Active power sharing

In [38] a criterion on the frequency droop gains and setpoints has been derived such that the generation units share the active power according to their power ratings. This is a desired control goal in many applications. However, it has been argued in [7] that system operators may not always seek to achieve a power sharing in proportion to the power ratings of the units. Instead they may also wish to take into account other technical, economic or environmental criteria, such as fuel consumption, generation costs or emission costs, see also [19].

In this regard, the ideas derived in [38] are easily applied to proportional active power sharing with respect to a user–defined criterion – also under the presence of conductances in the network. It turns out that the same criterion ensures that storage devices in charging mode, *i.e.* $P_i^d < 0$ for some $i \in \bar{n}$, are charged proportionally. To formulate the selection criterion for the controller gains and setpoints, we employ the following definition.

Definition 6.1. *Let $\chi_i \in \mathbb{R}_{>0}$ denote weighting factors and P_i^s the steady–state active power flow, $i \sim \bar{n}$. Then two inverters at nodes i and k are said to share their active powers proportionally if*

$$\frac{P_i^s}{\chi_i} = \frac{P_k^s}{\chi_k}. \tag{40}$$

A possible choice for χ_i would be, for example, $\chi_i = S_i^N$, $i \sim \bar{n}$. However, the weighting factors χ_i, $i \sim \bar{n}$, do not have to be equal for all inverters, *i.e.* active power could be shared according to economic or environmental criteria by some inverters, while it could be shared according to the power ratings by other inverters.

Lemma 6.2. *Consider the system (9), (1). Assume that it possesses a synchronized motion with synchronization frequency $\omega^s \in \mathbb{R}$. Then all inverters the power outputs of which satisfy $\mathrm{sign}(P_i^s) = \mathrm{sign}(P_k^s)$, achieve proportional active power sharing if the gains k_{P_i} and k_{P_k} and the active power setpoints P_i^d and P_k^d are chosen such that*

$$k_{P_i}\chi_i = k_{P_k}\chi_k \text{ and } k_{P_i}P_i^d = k_{P_k}P_k^d, \tag{41}$$

$i \sim \bar{n}$ and $k \sim \bar{n}$.

Proof. The claim follows in a straightforward manner from [38], where it has been shown for first–order inverter models and $\chi_i = S_i^N$, $P_i^d > 0$, $P_i^s > 0$, $i \sim \bar{n}$. Under conditions (41) we have, along the synchronized motion,

$$\frac{P_i^s}{\chi_i} = \frac{-\omega^s + \omega^d + k_{P_i}P_i^d}{k_{P_i}\chi_i} = \frac{-\omega^s + \omega^d + k_{P_k}P_k^d}{k_{P_k}\chi_k} = \frac{P_k^s}{\chi_k},$$

where $i \in \bar{n}$ and $k \in \bar{n}$ with $\mathrm{sign}(P_i^s) = \mathrm{sign}(P_k^s)$. □□□

Remark 6.3. The conditions in Lemma 6.2 also imply that storage devices in charging mode are charged proportionally.

Remark 6.4. Note that proportional active power sharing is achieved by Lemma 6.2 independently of the admittance values of the network. However, in a highly ohmic network, the droop control laws (4) may induce high fluctuating currents due to the stronger coupling of phase angles and reactive power, see (1). Then, additional methods such as the virtual output impedance [17] or alternative droop control laws [43] could be employed instead of (4).

Remark 6.5. Condition (38) in Corollary 5.12 is satisfied if all gains k_{P_i} and all setpoints P_i^d, $i \sim \bar{n}$, are selected according to Lemma 6.2.

Remark 6.6. As described in Section 3, the voltage droop control law (4) follows a similar heuristic approach as the frequency control droop law, aiming at obtaining a desired reactive power distribution in a synchronized state. However, the conditions for proportional active power sharing in Lemma 6.2 are derived using the fact that the frequency of a synchronized motion is equal all over the network, *i.e.* $\omega_i^s = \omega_k^s = \ldots = \omega^s$, and serves thus as a common communication signal. This is not the case for the voltage, since, in general, $V_i^s \neq V_k^s$ for $i \in \bar{n}$, $k \in \bar{n}$. In the special case of equal voltage amplitudes, *i.e.* $V_i^s = V_k^s$, $i \in \bar{n}$, $k \in \bar{n}$, proportional reactive power sharing can be achieved by selecting $V_i^d = V_k^d$ as well as voltage droop gains k_{Q_i} and k_{Q_k} and setpoints Q_i^d and Q_k^d following Lemma 6.2. The fact that the voltage droop control (4) does, in general, not achieve proportional reactive power sharing has been widely recognized in the literature and several alternative or modified decentralized droop control structures have been proposed, *e.g.,* in [27, 42], with the purpose of improving the reactive power sharing. Nevertheless, proportional reactive power sharing is still a challenging open question.

7. Simulation example

The theoretical analysis is illustrated via simulation examples based on the three–phase islanded Subnetwork 1 of the CIGRE benchmark medium voltage distribution network [33]. The network is a meshed network and consists of 11 main buses, see Fig. 1.

The following two modifications are made compared to the original system given in [33]: first, at bus 9b the combined heat and power (CHP) diesel generator is replaced by an inverter–interfaced CHP fuel cell (FC). Second, since the original network given in [33] stems from a distribution network connected to a transmission system, the power ratings of the generation units are scaled by a factor 4 compared to [33], such that the controllable units (CHPs, batteries, FC) can satisfy the load demand in autonomous operation mode at least during some period of time.

The network in Fig. 1 possesses a total of six controllable generation sources of which two are batteries at buses 5b ($i = 1$) and 10b ($i = 5$), two are FCs in households at buses 5c ($i = 2$) and 10c ($i = 6$) and two are FC CHPs at buses 9b ($i = 3$) and 9c ($i = 4$). We assume that all controllable generation units are equipped with frequency and voltage droop control as given in (4). We associate to each inverter its power rating S_i^N, $i \in \bar{n}$. Since the apparent power ratings of the generation sources are not specified in [33], we set S_i^N to the maximum active power given for each source in Table 2 of [33]. The transformer impedances of the inverter–interfaced units are modeled based on the IEEE standard 399–1997 [21]. For simplicity, we assume that the transformer power rating is equivalent to the power rating of the corresponding inverter S_i^N, $i \in \bar{n}$.

Non–controllable PV units are connected at buses 3, 4, 6, 8 and 11. The loads at nodes 3–11 represent industrial and household loads as specified in Table 1 of [33], besides the load at node 1, which is neglected. The line parameters and lengths are as given in Table 3 of [33]. The total length of the lines is approximately 15 km.

All simulations are carried out in Plecs [31]. Compared to the model given by (1) and (9) used for the analysis, the inductances are represented by first–order ODEs in the model used for the simulations rather than constants as in (1). Hence, the simulations also serve to evaluate the validity of the model (9), (1), as well as the robustness of the stability condition (31) with respect to model uncertainties.

We consider the following two scenarios.

1) Lossless scenario. All loads and uncontrollable generation sources (PV, wind turbine) of the test system given in Fig. 1 are neglected. As outlined in Section 5, we merge the transformer and filter impedances of the inverters with the line impedances. The largest R/X ratio of an admittance in the network is then 0.30. For HV transmission lines it is typically 0.31 [10]. Hence, the assumption of dominantly inductive admittances is satisfied. Consequently, the droop control laws given in (4) are adequate and our stability analysis of Section 5 applies.

The batteries at nodes 5b and 10b are operated in charging mode, hence functioning as loads. We design the frequency droop gains and setpoints of the inverters according to Lemma 6.2 with $\chi_i = S_i^N$, $P_i^d = \alpha_i S_i^N$ pu and $k_{P_i} = 0.2/S_i^N$ Hz/pu for all $i \in \bar{n}$, where pu denotes per unit values with respect to the common system base power S_{base} given in Table 1. Hence, the inverters should supply the requested power, respectively be charged, in proportion to their power ratings. We assume the power setpoints have been provided by some sort of high–level control or energy management system, see Remark 3.1, with $\alpha_i = 0.3$ for inverters in generation mode ($i = 2, 3, 4, 6$) and $\alpha_i = -0.4$ for inverters in charging mode, *i.e.* $i = 1, 5$.

The reactive power setpoints are set to $Q_i^d = \beta_i S_i^N$ pu with $\beta_i = 0.025$ for all $i \in \bar{n}$ to account for the inductive behavior of the lines. The voltage droop gains are chosen in the same relation as the frequency droop gains, *i.e.* $k_{Q_i} = 0.1/S_i^N$ pu/pu and $V_i^d = 1$ pu for all $i \in \bar{n}$. The low pass filter time constants are set to $\tau_{P_i} = 0.5$ s, $i \sim \bar{n}$. The main system data and control gains are given in Table 1.

The simulation results are shown in Fig. 2. After a transient the frequencies synchronize and the voltage amplitudes become constant. The latter satisfy the usual requirement of $0.9 < V_i^s < 1.1$ for V_i^s in pu and $i \sim \bar{n}$. The initial conditions have been chosen arbitrarily. Condition (31) is satisfied and hence the synchronized motion is locally asymptotically stable.

Furthermore, the batteries are charged in proportion to their power ratings with the active power also being supplied proportionally, as stated in Lemma 6.2. Hence, the simulation confirms that the frequency droop control, as given in (4), is suited to achieve the desired objective of active power sharing. But, as discussed in Section 6, the reactive power is not shared proportionally, limiting the overall performance of the voltage droop control law (4).

Our experience in numerous simulations with large variety of control gains, setpoints, low pass filter time constants and initial conditions is that whenever the solutions of the system converge to a synchronized motion as defined in Assumption 5.4, the latter is locally asymptotically stable by condition (31). However, there exist gain settings such that the solutions of the system exhibit limit–cycle behavior. As one would expect, this is the case for very large control gains and low pass filter time constants.

2) Scenario with constant impedance loads. In this simulation scenario the robustness of the stability condition (31) with respect to loads represented by constant impedances is evaluated.

It is therefore assumed that all PV units work at 50% of their nominal power with $\cos(\phi) := P/S = 0.98$ and are treated as negative loads, while the wind turbine is not generating any power.

The corresponding admittance representing a load at a node is computed at nominal frequency and voltage and by adding the load demand and the non–controllable gen-

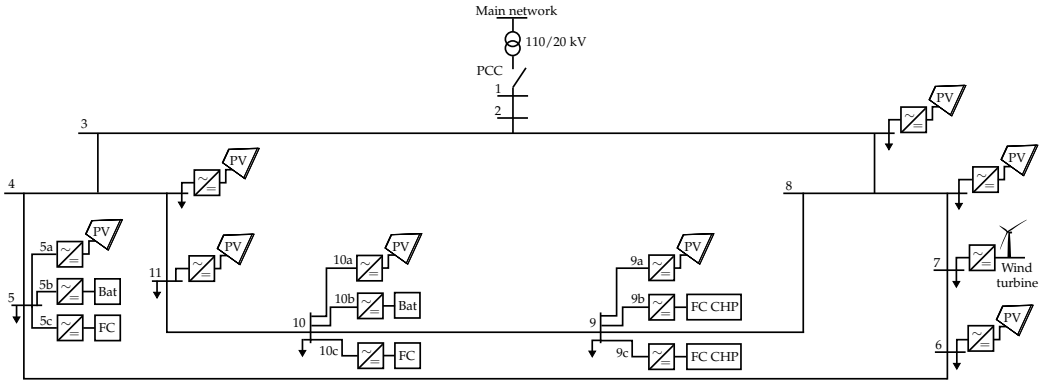

Figure 1: 20 kV MV benchmark model adapted from [33] with 11 main buses and inverter–interfaced units of type: PV–Photovoltaic, FC–fuel cell, Bat–battery, FC CHP–combined heat and power fuel cell. PCC denotes the point of common coupling to the main grid. The sign ↓ denotes loads. The numbering of the main buses is according to [33].

eration at each node. Then, in the corresponding Kron–reduced network all nodes represent controllable DGs.

At first, the admittance matrix of the equivalent Kron–reduced network is computed. As in the lossless scenario, the largest R/X ratio is 0.30. Thus, the assumption of dominantly inductive admittances is also satisfied in the presence of impedances representing loads. The control gains are chosen as specified in the lossless scenario with $\alpha_i = 0.6$ and $\beta_i = 0.25$, $i = 1, \ldots, 6$. Hence, all inverters operate in generation mode. The voltage setpoints and low pass filter time constants are as in the lossless case. We again assume the power setpoints have been provided by some sort of high–level control or energy management system. The main data are given in Table 2.

The simulation results are displayed in Fig. 3. All trajectories converge to a synchronized motion satisfying condition (31), indicating that the condition is robust – to a certain extent – to the presence of transfer and load conductances. The inverters share the active power demand of the loads as stated in Lemma 6.2. Compared to the lossless scenario, all inverters provide positive reactive power. However, as in the lossless scenario, the reactive power sharing is not proportional among all units since in steady–state the voltage amplitudes are not equal at all buses.

Furthermore, numerous simulations with different parameters indicate that the stability condition (31) is satisfied in all cases in which the solutions of the system converge to a synchronized motion. As in the lossless case, there are gain settings such that the solutions of the system do not converge to a desired synchronized motion as defined in Assumption 5.4, but show a limit cycle behavior. This is typically the case for very large control gains and/or large low pass filter time constants.

Table 1: Test system parameters for the lossless scenario, $i = 1, \ldots, 6$.

Base values	$S_{\text{base}} = 4.75$ MVA, $V_{\text{base}} = 20$ kV
S_i^N	$[0.505, 0.028, 0.261, 0.179, 0.168, 0.012]$ pu
P_i^d	$[-0.202, 0.008, 0.078, 0.054, -0.067, 0.004]$ pu
k_{P_i}	$[0.396, 7.143, 0.766, 1.117, 1.191, 16.667]$ $\frac{\text{Hz}}{\text{pu}}$
Q_i^d	$[0.013, 0.001, 0.007, 0.005, 0.004, 0.000]$ pu
k_{Q_i}	$[0.198, 3.571, 0.383, 0.559, 0.595, 8.333]$ $\frac{\text{pu}}{\text{pu}}$

Table 2: Test system parameters for the lossy scenario with loads represented by constant impedances, $i = 1, \ldots, 6$.

Base values	$S_{\text{base}} = 4.75$ MVA, $V_{\text{base}} = 20$ kV
Max. sys. load	0.91+j0.30 pu
Total PV gen.	0.15 pu
S_i^N	$[0.505, 0.028, 0.261, 0.179, 0.168, 0.012]$ pu
P_i^d	$[0.303, 0.017, 0.157, 0.107, 0.101, 0.007]$ pu
k_{P_i}	$[0.396, 7.143, 0.766, 1.117, 1.191, 16.667]$ $\frac{\text{Hz}}{\text{pu}}$
Q_i^d	$[0.126, 0.007, 0.065, 0.045, 0.042, 0.003]$ pu
k_{Q_i}	$[0.198, 3.571, 0.383, 0.559, 0.595, 8.333]$ $\frac{\text{pu}}{\text{pu}}$

8. Conclusions and future work

We have considered the problems of frequency stability, voltage stability and power sharing in droop–controlled inverter–based microgrids. First, we have shown that the trajectories of the system are globally bounded for all practical choices of controller gains and setpoints. We then have derived a sufficient condition for local stability for a lossless microgrid using a port–Hamiltonian representation of the latter. The condition states that local stability is independent of the choice of the controller gains and setpoints of the frequency droop controller as well as of the low pass filter time constants, but does depend on the choice of the controller gains and setpoints of the voltage droop controller.

The asymptotic stability property is established con-

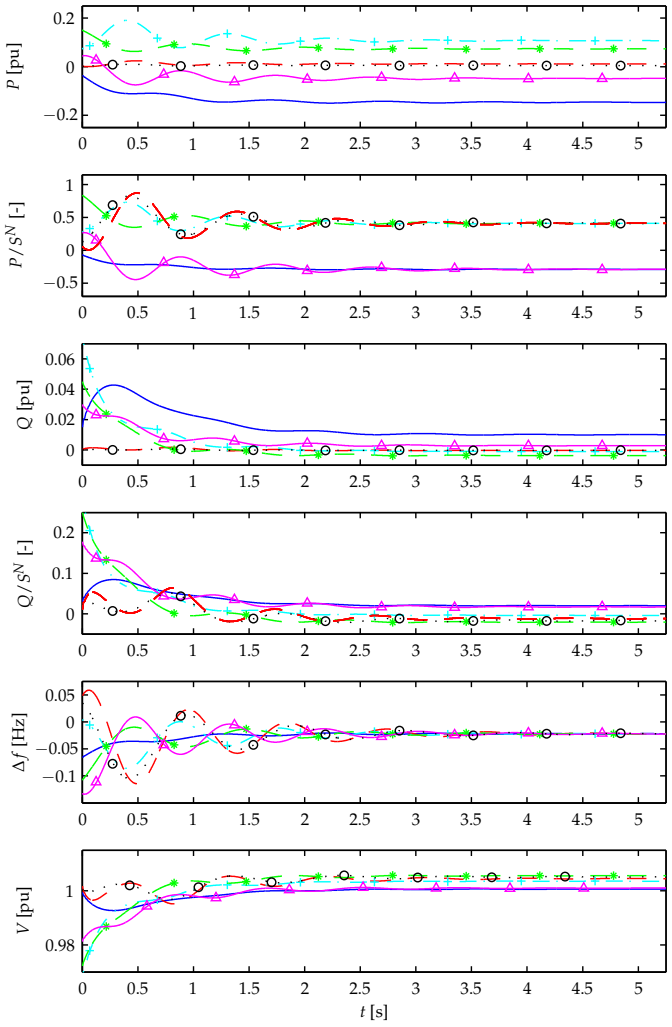

Figure 2: Lossless scenario. Trajectories of the power outputs P_i and Q_i in pu, the power outputs relative to source rating P_i/S_i^N and Q_i/S_i^N, the internal relative frequencies $\Delta f_i = (\omega_i - \omega^d)/(2\pi)$ in Hz and the voltage amplitudes V_i in pu of the controllable sources in the microgrid given in Fig. 1, $i = 1, \ldots, 6$. The active power is shared by the generating sources in proportion to their ratings in steady–state, i.e $P_i^s/S_i^N = P_k^s/S_k^N$ for $i, k = 2, 3, 4, 6$, while the batteries are charged in proportion to their ratings, *i.e.* $P_1^s/S_1^N = P_5^s/S_5^N$. The lines correspond to the following sources: battery 5b, $i = 1$ '–', FC 5c, $i = 2$ '- -', FC CHP 9b, $i = 3$ '+-', FC CHP 9c, $i = 4$ '* -', battery 10b, $i = 5$ '△ -' and FC 10c, $i = 6$ 'o-'. The initial conditions have been chosen arbitrarily. All trajectories converge to a locally aymptotically stable synchronized motion satisfying condition (31). The voltage amplitudes remain within 1 ± 0.1 pu in steady–state.

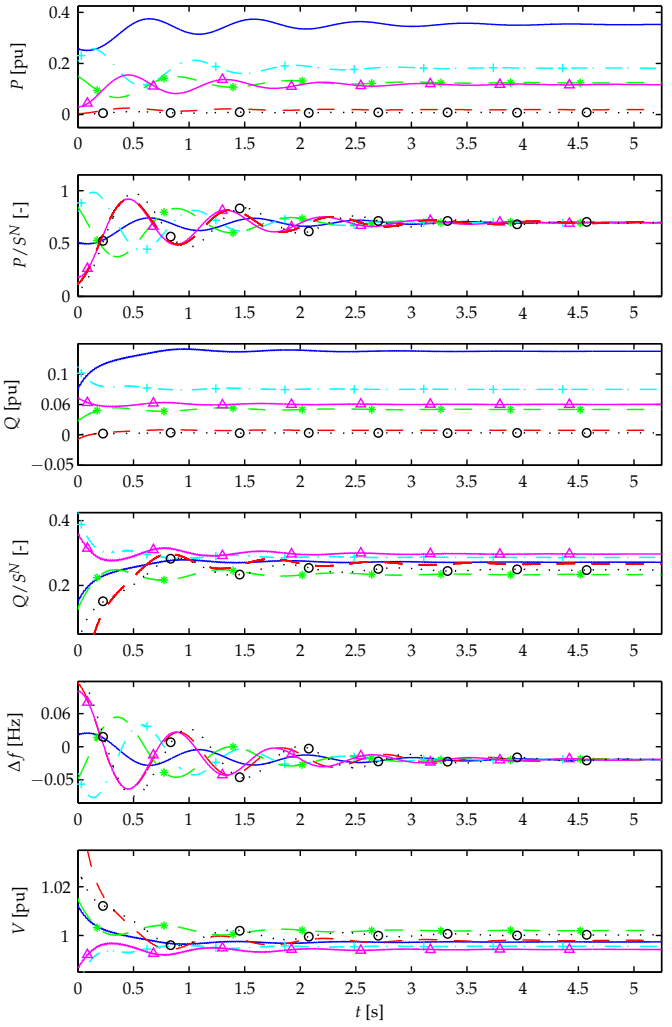

Figure 3: Scenario with constant impedance loads. Trajectories of the power outputs P_i and Q_i in pu, the power outputs relative to source rating P_i/S_i^N and Q_i/S_i^N, the internal relative frequencies $\Delta f_i = (\omega_i - \omega^d)/(2\pi)$ in Hz and the voltage amplitudes V_i in pu of the controllable sources in the microgrid given in Fig. 1, $i = 1, \ldots, 6$. The active power is shared by the sources in proportion to their ratings in steady–state, i.e $P_i^s/S_i^N = P_k^s/S_k^N$ for all $i, k = 1, \ldots, 6$. The lines correspond to the following sources: battery 5b, $i = 1$ '–', FC 5c, $i = 2$ '- -', FC CHP 9b, $i = 3$ '+-', FC CHP 9c, $i = 4$ '* -', battery 10b, $i = 5$ '△ -' and FC 10c, $i = 6$ 'o-'. The initial conditions have been chosen arbitrarily. All trajectories converge to a synchronized motion satisfying condition (31) indicating that the condition is robust – to a certain extent – to the presence of transfer and load conductances.

structing a *bona fide* Lyapunov function – alas, a non–strict one. However, converse Lyapunov theorems ensure the existence of a strict Lyapunov function, from which some robustness properties can be inferred. A case of particular interest, which is currently under investigation, is robustness in the presence of conductances. Two additional contributions of the paper are a selection of controller gains that relaxes some condition of the local stability result and, at the same time, ensures that the desired active power distribution is achieved in steady–state.

The theoretical analysis has been illustrated via simulation examples based on the the CIGRE benchmark MV distribution network. The derived stability condition is satisfied and a desired steady–state active power distribution is achieved in simulation for a wide selection of different control gains, setpoints, low pass filter time constants and initial conditions.

The simulations also show that, despite the observation that meshed microgrids with droop control possess a locally stable synchronized motion for a wide range of control gains, the conventional voltage droop control does, in general, not guarantee proportional reactive power sharing.

Therefore, future work concerns – possibly distributed – control solutions for accurate reactive power sharing, while guaranteeing network stability. Another interesting, and challenging, open problem is power sharing and stability in dominantly resistive microgrids.

Acknowledgements

The authors would like to thank F. Dörfler for many helpful comments on the topics of this paper. Partial support from the HYCON2 Network of excellence (FP7 ICT 257462) is also acknowledged.

References

[1] Barklund, E., Pogaku, N., Prodanovic, M., Hernandez-Aramburo, C., & Green, T. (2008). Energy management in autonomous microgrid using stability-constrained droop control of inverters. *IEEE Transactions on Power Electronics*, *23*, 2346 –2352.

[2] Bretas, N., & Alberto, L. F. C. (2003). Lyapunov function for power systems with transfer conductances: extension of the invariance principle. *IEEE Transactions on Power Systems*, *18*, 769–777.

[3] Chandorkar, M., Divan, D., & Adapa, R. (1993). Control of parallel connected inverters in standalone AC supply systems. *IEEE Transactions on Industry Applications*, *29*, 136 –143.

[4] Coelho, E., Cortizo, P., & Garcia, P. (2002). Small-signal stability for parallel-connected inverters in stand-alone AC supply systems. *IEEE Transactions on Industry Applications*, *38*, 533 –542.

[5] Davy, R. J., & Hiskens, I. A. (1997). Lyapunov functions for multimachine power systems with dynamic loads. *IEEE Transactions on Circuits and Systems I: Fundamental Theory and Applications*, *44*, 796–812.

[6] De Brabandere, K., Bolsens, B., Van den Keybus, J., Woyte, A., Driesen, J., & Belmans, R. (2007). A voltage and frequency droop control method for parallel inverters. *IEEE Transactions on Power Electronics*, *22*, 1107 –1115.

[7] Diaz, G., Gonzalez-Moran, C., Gomez-Aleixandre, J., & Diez, A. (2010). Scheduling of droop coefficients for frequency and voltage regulation in isolated microgrids. *IEEE Transactions on Power Systems*, *25*, 489 –496.

[8] Dib, W., Ortega, R., Barabanov, A., & Lamnabhi-Lagarrigue, F. (2009). A globally convergent controller for multi-machine power systems using structure-preserving models. *IEEE Transactions on Automatic Control*, *54*, 2179 –2185.

[9] Dörfler, F., & Bullo, F. (2012). Synchronization and transient stability in power networks and non-uniform Kuramoto oscillators. *SIAM Journal on Control and Optimization*, *50*, 1616–1642.

[10] Engler, A. (2005). Applicability of droops in low voltage grids. *International Journal of Distributed Energy Resources*, *1*, 1–6.

[11] Farhangi, H. (2010). The path of the smart grid. *IEEE Power and Energy Magazine*, *8*, 18 –28.

[12] Glover, J. D., Sarma, M. S., & Overbye, T. J. (2011). *Power system analysis and design*. Cengage Learning.

[13] Godsil, C., & Royle, G. (2001). *Algebraic Graph Theory*. Springer.

[14] Guedes, R., Silva, F., Alberto, L., & Bretas, N. (2005). Large disturbance voltage stability assessment using extended lyapunov function and considering voltage dependent active loads. In *IEEE PESGM* (pp. 1760–1767).

[15] Guerrero, J., Loh, P., Chandorkar, M., & Lee, T. (2013). Advanced control architectures for intelligent microgrids – part I: Decentralized and hierarchical control. *IEEE Transactions on Industrial Electronics*, *60*, 1254–1262.

[16] Guerrero, J., Matas, J., de Vicuna, L. G., Castilla, M., & Miret, J. (2007). Decentralized control for parallel operation of distributed generation inverters using resistive output impedance. *IEEE Transactions on Industrial Electronics*, *54*, 994 –1004.

[17] Guerrero, J., Garcia de Vicuna, L., Matas, J., Castilla, M., & Miret, J. (2005). Output impedance design of parallel-connected UPS inverters with wireless load-sharing control. *IEEE Transactions on Industrial Electronics*, *52*, 1126 – 1135.

[18] Hatziargyriou, N., Asano, H., Iravani, R., & Marnay, C. (2007). Microgrids. *IEEE Power and Energy Magazine*, *5*, 78 –94.

[19] Hernandez-Aramburo, C., Green, T., & Mugniot, N. (2005). Fuel consumption minimization of a microgrid. *IEEE Transactions on Industry Applications*, *41*, 673 – 681.

[20] Horn, R. A., & Johnson, C. R. (2012). *Matrix analysis*. Cambridge university press.

[21] IEEE (1998). IEEE recommended practice for industrial and commercial power systems analysis (brown book). *IEEE Standard 399-1997*, (pp. 1–488).

[22] Khalil, H. K. (2002). *Nonlinear systems* volume 3. Prentice Hall.

[23] Kundur, P. (1994). *Power system stability and control*. McGraw-Hill.

[24] Kundur, P., Paserba, J., Ajjarapu, V., Andersson, G., Bose, A., Canizares, C., Hatziargyriou, N., Hill, D., Stankovic, A., Taylor, C., Van Cutsem, T., & Vittal, V. (2004). Definition and classification of power system stability IEEE/CIGRE joint task force on stability terms and definitions. *IEEE Transactions on Power Systems*, *19*, 1387–1401.

[25] Lasseter, R. (2002). Microgrids. In *IEEE Power Engineering Society Winter Meeting, 2002* (pp. 305 – 308 vol.1). volume 1.

[26] Lasseter, R. H. (2011). Smart distribution: Coupled microgrids. *Proceedings of the IEEE*, *99*, 1074–1082.

[27] Li, Y. W., & Kao, C.-N. (2009). An accurate power control strategy for power-electronics-interfaced distributed generation units operating in a low-voltage multibus microgrid. *IEEE Transactions on Power Electronics*, *24*, 2977 –2988.

[28] Lopes, J., Moreira, C., & Madureira, A. (2006). Defining control strategies for microgrids islanded operation. *IEEE Transactions on Power Systems*, *21*, 916 – 924.

[29] Ortega, R., Galaz, M., Astolfi, A., Sun, Y., & Shen, T. (2005). Transient stabilization of multimachine power systems with nontrivial transfer conductances. *IEEE Transactions on Automatic Control*, *50*, 60 – 75.

[30] Ortega, R., van der Schaft, A., Maschke, B., & Escobar, G. (2002). Interconnection and damping assignment passivity-based control of port-controlled Hamiltonian systems. *Automatica*, *38*, 585–596.

[31] Plexim GmbH (2013). Plecs software, www.plexim.com.

[32] Pogaku, N., Prodanovic, M., & Green, T. (2007). Modeling, analysis and testing of autonomous operation of an inverter-based microgrid. *IEEE Transactions on Power Electronics*, *22*, 613 –625.

[33] Rudion, K., Orths, A., Styczynski, Z., & Strunz, K. (2006). Design of benchmark of medium voltage distribution network for investigation of DG integration. In *IEEE PESGM*.

[34] van der Schaft, A. (2000). *L2-Gain and Passivity Techniques in Nonlinear Control*. Springer.

[35] Schiffer, J., Anta, A., Trung, T. D., Raisch, J., & Sezi, T. (2012). On power sharing and stability in autonomous inverter-based microgrids. In *Proc. 51st IEEE CDC* (pp. 1105–1110). Maui, HI, USA.

[36] Schiffer, J., Goldin, D., Raisch, J., & Sezi, T. (2013). Synchronization of droop-controlled microgrids with distributed rotational and electronic generation. In *Proc. 52nd IEEE CDC* (pp. 2334–2339). Florence, Italy.

[37] Schiffer, J., Ortega, R., Astolfi, A., Raisch, J., & Sezi, T. (2014). Stability of synchronized motions of inverter–based microgrids under droop control. To appear at IFAC World Congress, Cape Town, South Africa.

[38] Simpson-Porco, J. W., Dörfler, F., & Bullo, F. (2013). Synchronization and power sharing for droop-controlled inverters

in islanded microgrids. *Automatica*, *49*, 2603 – 2611.

[39] Simpson-Porco, J. W., Dörfler, F., & Bullo, F. (2013). Voltage stabilization in microgrids using quadratic droop control. In *Proc. 52nd IEEE CDC* (pp. 7582–7589). Florence, Italy.

[40] Soultanis, N. L., Papathanasiou, S. A., & Hatziargyriou, N. D. (2007). A stability algorithm for the dynamic analysis of inverter dominated unbalanced LV microgrids. *IEEE Transactions on Power Systems*, *22*, 294 –304.

[41] Varaiya, P., Wu, F. F., & Chen, R.-L. (1985). Direct methods for transient stability analysis of power systems: Recent results. *Proceedings of the IEEE*, *73*, 1703–1715.

[42] Yao, W., Chen, M., Matas, J., Guerrero, J., & Qian, Z.-M. (2011). Design and analysis of the droop control method for parallel inverters considering the impact of the complex impedance on the power sharing. *IEEE Transactions on Industrial Electronics*, *58*, 576 –588.

[43] Zhong, Q.-C. (2013). Robust droop controller for accurate proportional load sharing among inverters operated in parallel. *IEEE Transactions on Industrial Electronics*, *60*, 1281–1290.